ALCOHOL REACTION KINETICS ON COPPER/ZINC OXIDE SURFACE

D. L. Roberts, L. Chan, and G. L. Griffin

Department of Chemical Engineering
and Materials Science
University of Minnesota
Minneapolis, Minnesota 55455

ABSTRACT

Recent commercial and academic interest in CH_3OH synthesis via CO hydrogenation, together with the high selectivity and relative simplicity of this reaction, make it an ideal reaction for testing and comparing adsorption studies, proposed mechanisms, and macroscopic rate behavior for oxide-based catalysts. Adsorption studies of H_2, H_2O, and CH_3OH on ZnO powders and model thin films of Cu/ZnO have resolved several discrete adsorption sites. Infrared and temperature programmed decomposition studies of adsorbed CH_3OH are used to determine the energetics of the $CH_3O_{(a)}$ and $HCOO_{(a)}$ decomposition steps at these sites. Comparative studies using model Cu/ZnO thin films have resolved features common to bulk ZnO and bulk Cu, as well as differences in behavior which can be attributed to the availability of ZnO lattice anions at the perimeter of the Cu clusters. The results suggest that Type I sites on ZnO do not have a major role in the CH_3OH synthesis reaction on Cu/ZnO catalysts. Instead, the CH_3OH reaction may occur preferentially at perimeter sites of Cu clusters.

INTRODUCTION

The reactivity of carbon-oxygen bonds in adsorbed oxygenated hydrocarbon intermediates is of fundamental importance in understanding the rates and selectivity of alcohol reactions on heterogeneous catalysts. Reactions of commerical interest include methanol synthesis, the direct synthesis of higher alcohols, alcohol decomposition (e.g., reforming, partial oxidation), etherification (e.g., production of MTBE as a gasoline blending agent), condensation (e.g., conversion to C-8 compounds on zeolites or other acid catalysts), and functionalization (e.g., amination reactions).

Work in our laboratory has focussed on understanding the surface reactions involved in the catalytic formation and decomposition of the simplest alcohol, CH_3OH. In particular, we have undertaken a systematic study of a series of model ZnO or Cu/ZnO catalyst surfaces using a combination of infrared spectroscopy, temperature programmed desorption and decomposition of adsorbates, and reactor measurements of transient and/or steady state kinetics. These studies are aimed at identifying the composition and geometry of various adsorption sites on the Cu/ZnO surface, the mechanism and kinetics of adsorbate reactions at the sites, and the importance of each site in the overall CH_3OH synthesis reaction.

In the present paper we describe selected results from our overall program. These results are chosen to illustrate two points: The importance of the formate intermediate in alcohol reactions on oxide surfaces and its role in maintaining hydrogenation selectivity, and the relative importance of adsorption sites on the

ZnO and Cu components of the catalyst surface.

EXPERIMENTAL

Comparative studies of high surface area powders and planar thin-film samples are performed in two independent apparatus. Studies of powder samples were performed in the IR-TPD cell shown in Fig. 1. The sample containing 50-100 mg of ZnO is deposited from an aqueous slurry onto the front face of the cell mirror, a silver disk which is soldered to the re-entrant inner wall of the cell body. The mirror disk can be heated using the attached cartridge heater, or cooled to 100 K by flowing cooled N_2 through the attached coolant tube. After sealing the front of the cell using a flange-mounted CaF_2 window, the cell is attached to a stainless steel gas handling system and positioned inthe sample compartment of the FTIR spectrometer (Nicolet 60-SX). Spectra are obtained in a two-pass tranmission mode by reflecting the IR beam from the mirror disk, thereby passing through the sample layer twice. During a typical in-situ TPD experiment, IR spectra are recorded at regular temperature intervals (75 scans/spectrum, at a scan rate of 1-2 scans/sec; resolution = 8 cm^{-1}), while the flux of each desorbing species is monitored using a quadrupole mass spectrometer (Spectramass 800) attached to the gas handling system. All of the TPD experiments described here were performed with the IR-TPD cell evacuated and pumped by the gas handling system (i.e., no carrier gas is used).

The majority of the results described below were obtained using Kadox 25 ZnO, in order to examine the possible importance of the unique Type I adsorption sites for H_2 that have been reported for this material. The pretreatment required to activate the Type I sites involves (step 1) heating the sample in vacuum ($P < 10^{-6}$ torr) at 673 K for 3 hours, (step 2) cooling to 573 K and admitting 0.5 torr O_2 for 10 minutes, then evacuating (O_2 cycle repeated three times), and (step 3) re-heating in vacuum to 673 K for 20 minutes before cooling to room temperature.

Once the pretreatment steps were finished, the IR-TPD experiments for the adsorbate of interest could be repeated indefinitely. For experiments using CH_3OH and H_2O, both of which are irreversibly adsorbed at 300 K, a volumetrically determined amount of either gas is admitted from the gas handling system into the sample cell. For H_2 adsorption experiments, it is necessary to fill the sample cell with 40 torr H_2 at 300 K to occupy the Type I sites, since the Type I H_2 adsorption state desorbs readily at room temperature.

The complementary experiments using planar samples were performed in the apparatus shown schematically in Fig. 2. The sample configuration is shown schematically in the inset of the figure. Samples are prepared by first depositing thin films of ZnO onto Au substrates, using a separate RF plasma sputtering system (perkin Elmer model 2400) with a ZnO target and a background gas of 24% O_2 : 76% Ar at a pressure of 1 Pa. The ZnO deposition rate was 200 A/min and the deposited film thickness was approximately 1 μm. X-ray diffraction measurements confirm that the film grains are preferentially oriented with their c-axis within 5° of the surface normal. Thus the films expose a high-fraction of (0001)-Zn planes and/or vicinal defect surfaces.

After the ZnO film has been deposited, a chromel-alumel thermocouple is attached to the Au substrate and the sample is mounted into the TPD apparatus shown in the main part of Fig. 2. The apparatus consists of an ion-pumped stainless-steel bell jar equipped with a single pass cylindrical mirror analyzer, a quadrupole mass spectrometer, an ion sputtering gun, a side chamber which contains a Cu evaporation source and a quartz film thickness monitor. The sample itself is mounted on a differentially pumped sliding seal transfer rod that

permits the sample to be translated between the evaporation chamber and the focal point of the CMA.

Two sequences are used to prepare sufaces with different Cu loadings. In most cases, the loading was controlled by changing the exposure time of a sputter cleaned ZnO surface to the Cu evaporant flux. The deposition flux was approximately A/min, as measured using the film thickness monitor. The sample temperature during evaporation is 300 K. An independent measure of the Cu coverage is obtained using Auger analysis to examine the surface after evaporation. For a few experiments, an alternate procedure for varying the Cu loading consists of initially evaporating a high coverage of Cu and then heating the sample progressively higher temperatures above 800 K to desorb increasing amounts of the initial Cu layer.

After recording the Auger spectrum of the surface following Cu evaporation, methanol decomposition experiments were performed by exposing the sample to CH_3OH at 300 K by backfilling the chamber. After the background pressure returned to ca. 10^{-10} torr, the sample is heated and the evolved products are monitored using the mass spectrometer. The heating rate used for the thin film experiments is 25 K/sec. Care is taken to stop each TPD experiment at a low enough temperature (ca 750 K) to prevent any loss of Cu by re-evaporation. Spectra for each of the observed products are usually recorded separately in repetitive experiments. Reproducibility between experiments is confirmed periodically by using multiplexed signal acquisition, at a cost in signal resolution. Reproducibility can also be confirmed by comparing the record of total pressure vs. time measured by the ionization gauge in the main chamber.

RESULTS

Porous sample studies: Role of Type I sites. In Fig. 3 we show the IR spectra acquired during the adsorption and subsequent TPD of CH_3OH on Type I activated ZnO. The bottom curve is the spectrum of the sample in the presence of 40 torr H_2 at 300 K, obtained prior to absorbing CH_3OH. The sharp band at 1709 cm^{-1} and the less intense band at 3491 cm^{-1} correspond to the Zn-H and O-H stretching vibrations, respectively, which are characteristic of H_2 adsorbed at Type I sites. We note that the band observed at 3618 cm^{-1} is attributed to a residual surface $OH_{(S)}$ species and is not associated with Type I H_2 adsorption. Features in the 2900 to 2800 cm^{-1} region are due to residual surface hydrocarbon impurities still remaining after the three 573 K O_2 cleaning cycles of the pretreatment. The concentration of Type I sites in this sample is 5.8 μmole H_2/gm ZnO, as determined from the integrated area under an H_2 TPD spectrum.

The next curve is the spectrum obtained after evacuating the H_2 and adsorbing an about of CH_3OH corresponding to 10 μmole/gm. The bands appearing at 2932 and 2816 cm^{-1} are assigned to the asymmetric and symmetric C-H stretching vibrations of the surface methoxy species. We note that the adsorption of CH_3OH produces no new resolvable OH features in the region above 3500 cm^{-1}, nor does it perturb the residual surface OH band at 3618 cm^{-1}. If 40 torr of H_2 is admitted to the cell at this point, the Zn-H and O-H bands characteristic of Type I sites do not appear. This confirms that CH_3OH adsorbs irreversibly at Type I sites, blocking them from further H_2 adsorption. The fact that 10 μmole CH_3OH/gm ZnO are required to clock the sites completely indicates that some of the CH_3OH must be adsorbed at non-Type I sites, as well.

The next curve in Fig. 3 is the spectrum of the sample obtained t 530 K during the decomposition of the adsorbed CH_3OH. The intensity of the methoxy C-H bands at 2932 and 2816 cm^{-1} decreases, and new features grow in at 2875, 1574, 1364, 1377 cm^{-1}. These new bands are assigned respectively to the C-H stretching

mode, the asymmetric and symmetric O-C-O stretching modes, and the in-plane C-H bending mode of a surface $HCOO_{(a)}$ species. The asymmetric O-C-O stretching mode and the in-plane C-H bending mode also produce an additional combination band at 2965 cm^{-1}. These results deomonstrate the sequential conversion of $CH_3O_{(a)}$ species to $HCOO_{(a)}$ species.

A separate experiment was performed by interrupting the decomposition at 530 K (corresponding to the temperature at which the maximum $HCOO_{(a)}$ coverage is observed) and quickly cooling the sample to 300 K to preseve the surface $HCOO_{(a)}$ coverage. Admitting 40 torr of H_2 to the cell at this stage failed to produce IR bands at 3490 or 1710 cm^{-1}, thus indicating that the $HCOO_{(a)}$ species also block the Type I H_2 sites.

The uppermost curve is the spectrum of the sample obtained after completing the TPD experiment, cooling from 673 K to 300 K, adding 0.1 torr O_2 to improve the IR transmission, and then admitting 40 torr of H_2. The bands at 3492 and 1709 cm^{-1} have now been restored, indicating that the Type I sites have been made vacant following decomposition of the adsorbed CH_3OH.

The product desorption spectra recorded by the mass spectrometer during the preceeding experiment are shown in Fig. 4. The H_2 evolution curve has three resolvable features: a low temperature shoulder at 459 K, a broader shoulder hear 511 K, and a desorption maximum at 565 K. The H_2 desorption at 565 K is accompanied by the almost coincident desorption of CO and CO_2 at 573 K. In contrast, the H_2 evolved at 459 K and 511 K is not accompanied by any significant amount of carbon oxides. This is a clear indication that the H_2 evolution peaks at 459 K and 511 K are a result of the conversion of $CH_3O_{(a)}$, while the nearly simultaneous desorption of H_2, CO, and CO_2 at 565-573 K is due to the decomposition of the surface $HCOO_{(a)}$. Figure 4 also shows that H_2O is not a favored product of either $CH_3O_{(a)}$ conversion or $HCOO_{(a)}$ decomposition, despite the oxidized condition of the ZnO sample.

To determine the importance of Type I sites on ZnO for CH_3OH decomposition, we next performed a series of experiments using pre-adsorbed H_2O to block the Type I sites before adsorbing CH_3OH. Infrared spectra recorded in the presence of 40 torr of H_2 before and after H_2O was admitted to the cell showed that H_2O also adsorbs irreversibly into the Type I H_2 sites, blocking them from H_2 adsorption. Methanol was then admitted to the sample with the blocked Type I sites. Adsorption still occurs, as indicated by the IR spectrum which showed the C-H vibrational bands of the $CH_3O_{(a)}$ intermediate. The fact that CH_3OH dissociately adsorbed even on the Type I blocked sample confirms that CH_3OH adsorbs at non-Type I sites.

The TPD product desorption spectra recorded for the sample with co-adsorbed H_2O and CH_3OH are shown in Fig. 5. The first feature to note is the behavior of the H_2O desorption signal. A small amount of desorption is observed near 475 K; however, the majority of the H_2O desorbs with a peak maximum near 600 K. This is identical to the desorption behavior of pure H_2O (i.e., without co-adsorbed CH_3OH). This indicates that the H_2O molecules adsorbed in Type I sites retain their identity throughout the experiment, that the Type I sites remain blocked by H_2O throughout the temperature range of CH_3OH decomposition, and that the adsorbed H_2O is not consumed in the formation of CO_2 during the formate decomposition step.

A small amount of molecular CH_3OH desorbs between 400 K and 500 K. A similar molecular CH_3OH desorption peak can be observed from samples containing no pre-adsorbed H_2O, provided the initial CH_3OH coverage is greater than 10 μmole/gm. This indicates that there is a finite combined concentration of both Type I and non-Type I sites at which CH_3OH is dissociatively adsorbed. Additional CH_3OH beyond this amount is adsorbed into a less tightly bound state

which desorbs molecularly at 450 K. The low temperature shoulder in the H_2O desorption spectrum probably arises from a similar state.

Dissociatively adsorbed CH_3OH ultimately decomposes to yield H_2, CO, and CO_2. The H_2 evolution curve shows two resolved maxima at 493 K and 557 K, corresponding to the two highest temperature features in the H_2 desorption spectrum for decomposition of CH_3OH alone (cf. Fig. 4). However, the desorption shoulder at 459 K that was observed on the H_2O-free surface is absent! In addition, the H_2 desorption maximum at 493 K occurs without evolution of carbon oxides, while the H_2 maximum at 557 K is followed by the evolution of CO and CO_2 at 567 K and 581 K, respectively. Since the only difference between the experiments shown in Figs. 4 and 5 is the presence of pre-adsorbed H_2O in the Type I sites, we conclude that the H_2 peak at 493 K corresponds to the decomposition of surface methoxy species adsorbed at non-Type I sites, while the H_2 desorption feature observed at 459 K (on the H_2O-free surface) can be assigned to the decomposition of methoxy species adsorbed at Type I sites.

The decomposition of the remaining surface formate species gives rise to the H_2, CO, and CO_2 peaks between 557 and 581 K. The spread in temperature between the three species appears to be real, and may result from re-adsorption effects for CO and CO_2 which are more pronounced on samples with pre-adsorbed H_2O due to a short-lived re-generation of transient $HCOO_{(a)}$ species involving the adsorbed H_2O molecules. However, the desorption temperatures are similar to those observed in the absence of pre-adsorbed H_2O, indicating that the decomposition rate of the formate species is insensitive to Type I vs. non-Type I sites.

However, the CO_2:CO ratio is much greater than in the absence of pre-adsorbed H_2O. As noted above, this is not because pre-adsorbed H_2O at the Type I sites is incorporated into the CO_2 product. Instead, it appears that the decrease in CO intensity is a direct result of the blockage of Type I sites by H_2O. Thus we conclude that formate species produced at Type I sites decompose selectively to CO, while formate species at non-Type I sites decompose selectively to CO_2.

Thin film studies: Role of Cu sites. The product distribution resulting from CH_3OH decomposition on a clean, (0001) oriented ZnO thin film is shown in Fig. 6. The initial CH_3OH exposure is 5 L for each experiment (1 Langmuir = 10^{-6} torr sec). The observed product inlcude H_2, CH_2O, CO, and CO_2. We also looked for but did not observe desorption peaks for CH_4 and H_2.

Consistent with the results for ZnO powder described above, the spectra show that adsorbed CH_3OH decomposes in two well-resolved processes. The 585 K process corresponds to decomposition of the $CH_3O_{(a)}$ intermediate, and is characterized by the evolution of H_2 without CO or CO_2. The 585 K process also produces a small amount (ca. 20%) of desorbed CH_2O. The balance of the CH_2O is apparently stabilized immediatley, being converted to a formate precursor before it is able to desorb.

The 635 K process corresponds to the decomposition of $HCOO_{(a)}$ to produce H_2, CO, and a small amount of CO_2. Some additional CH_2O is also observed at 635 K, which may result either from the delayed decomposition of a limited number of $CH_3O_{(a)}$ species whose decompositon had been sterically impeded by occupied neighboring sites until 635 K. Alternatively, the CH_2O signal at 635 K may also result from the hydrogenation of a limited number of $HCOO_{(a)}$ species, using the $H_{(a)}$ atoms released by the decomposition of the remaining $HCOO_{(a)}$ species.

The apparent activation energies of the 585 K and 635 K processes are 35 and 38 kcal/mole, respectively, based on the Redhead equation for first-order decomposition kinetics and an assumed pre-exponential factor of 10^{13} sec^{-1}. These values are comparable to the activation energies for the $CH_3O(a)$ and

$HCOO_{(a)}$ decomposition steps computed for the powder experiments, i.e., 31 and 33 kcal/mole for the $CH_3O_{(a)}$ decomposition on Type I and non-Type I sites, respectively, and 40 kcal/mole for $HCOO_{(a)}$ decomposition. Comparision of the energies for $CH_3O_{(a)}$ decomposition on Type I vs. non-Type I sites suggests that Type I sites may in fact be absent from the Ar^+ ion sputtered and annealed ZnO thin film surfaces. We also note that the observation of CH_2O during the experiments on thin film ZnO samples is a result of the line-of-sight detection provided by the mass spectrometer when using a planar sample. Formaldehyde may also be produced initially during $CH_3O_{(a)}$ decomposition on powdered ZnO, but may not be detectable dur to irreversible re-adsorption on the pore walls before it can diffuse out of the powdered sample.

Figure 7 shows the product desorption spectra for CH_3OH decomposition on an evaporated Cu/ZnO sample. The Cu loading in this case is sufficient to decrease the Zn Auger signal to 35% of its clean-surface value. The CH_2O, H_2, CO, and CO_2 desorption features at 585 K and 635 K are still present, but are significantly attentuated. This indicates that CH_3OH decomposition is still occuring on ZnO sites, which implies that even at this high Cu loading, the Cu layer does not cover the ZnO surface uniformly.

Two differences from the decomposition behavior of clean ZnO are also observed. First, small H_2 and CH_2O desorption signals are observed near 410 K, and a small CO_2 peak is observed near 510 K. These features are quite similar to the CH_3OH decomposition behavior reported for metallic Cu[1]. This suggests that at least a portion of the evaporated Cu layer has agglomerated to form metallic Cu clusters, which are large enough to demonstrate the same CH_3OH decomposition behavior as bulk Cu.

The second difference is the large CO_2:CO ratio observed for the 635 K process. This is reminiscent of the $HCOO_{(a)}$ decomposition selectivity observed when H_2O was pre-adsorbed on powdered ZnO, and suggests that a portion of the evaporated Cu layer is sufficiently highly dispersed to perturb the decomposition selectivity of the $HCOO_{(a)}$ species on the ZnO surface. We cannot suggest a mechanism for this perturbation at this time.

As the final experiment described here, we sought to test the influence of surface oxidation state on the CH_3OH decompositon behavior of the evaporated Cu/ZnO thin film sample. Figure 8 shows the product desorption spectra for the same Cu/ZnO sample described above, following sequential exposure to 2 L of O_2 and 5 L of CH_3OH. Three main features are noted:

- The CO and CO_2 peaks at 635 K are unchanged from their intensities in the O_2-free case. However, the H_2 and CH_2O signals in the region of the 585 and 635 K decomposition processes have been essentially eliminated. Since pre-exposure to O_2 had no effect on the CH_3OH decomposition behavior of a clean ZnO thin film, this suggests that the dispersed Cu species proposed above also influence the O_2 adsorption character of the ZnO surface.
- The H_2 peak at 410 K is enhanced by a factor of two, relative to the case without pre-adsorbed O_2. The CH_2O peak at 410 K is also somewhat enhanced. This is consistent with earlier workers' results that pre-exposure to O_2 enhances the reactive sticking coefficient of CH_3OH on Cu surfaces, and indicates that this enhancement also occurs on the small Cu clusters present on the Cu/ZnO thin film studied here.
- The CO_2 peak at 510 K is greatly enhanced following O_2 pre-exposure. This result is also consistent with the behavior of metallic Cu, where adsorbed $O_{(a)}$ is expected not only to enhance dissociative CH_3OH adsorption but also to increase the conversion of $CH_3O_{(a)}$ to stable $HCOO_{(a)}$, which in turn is reported to decompose almost exclusively to CO_2.

Similar results to those described above were obtained for a series of Cu

loadings on ZnO thin films. In general, the low temperature decomposition processes at 410 K and 510 K were observed at every Cu loading. Interestingly, the enhancement effect of pre-adsorbed O_2 was observed only for higher Cu loadings. This it appears that metallic Cu clusters at the lowest loadings are small enough to activate dissociative CH_3OH adsorption without pre-adsorbed $O_{(a)}$. This may be the result of a spillover effect of dissociated $H_{(a)}$ atoms onto the ZnO support. For large clusters, the influence of the spillover effect would be limited to Cu atoms near the perimeter of the cluster, and the $O_{(a)}$ enhancement would be necessary to activate the remaining atoms in the cluster.

One other result is the fact that the method for preparing different Cu loadings had no effect on the CH_3OH decompositon behavior; i.e., samples prepared by progressive evaporation of increasing amounts of Cu behaved identically with samples prepared by successive heating of a high initial Cu loading to leave behind progressively decreasing amounts of Cu. We interpret this to indicate that both the cluster and dispersed Cu species are present in a thermodynamically equilibrated state.

DISCUSSION

Role of formate intermediates. The present results largely confirm our previous understanding that CH_3OH decomposition to CO or CO_2 occurs via the $CH_3O_{(a)}$ and $HCOO_{(a)}$ intermediates. For the powdered ZnO, we have shown that the selectivity of the $HCOO_{(a)}$ decomposition processes is sensitive to the geometry of the adsorption site: Type I sites yield CO as the major product, while non-Type I sites, possibly as a result of the presence of co-adsorbed H_2O, yield primarily CO_2. The effect of the dispersed Cu species on the Cu/ZnO thin film samples is also to increase the selectivity for $HCOO_{(a)}$ decomposition toward the CO_2 product. The latter result, of course, may also be due to a chemical effect, but it does serve to illustrate the role of the composition of the active site on the selectivity of elementary desorption or decomposition steps.

Our results using clean ZnO thin films also suggest for the first time the possibility that the $HCOO_{(a)}$ intermediate on the oxide surface may be hydrogenated to produce CH_2O (cf., the CH_2O desorption peak at 635 K in Fig. 6). Additional work is needed to eliminate the alternate explanation (i.e., the delayed decomposition of $CH_3O_{(a)}$ species due to neighboring site blockage), but together with the observation that CH_2O does not reach the mass spectrometer in the powdered ZnO experiments due to readsorption, this raises the possibility that the CH_3OH synthesis mechanism may involve discrete CO and CH_2O hydrogenation steps, with gas phase CH_2O as a short-lived intermediate present at low concentrations.

Role of Type I sites vs. Cu. The IR spectra in Fig. 3 clearly demonstrate that CH_3OH adsorbs dissociately at Type I sites. The site blocking experiments using pre-adsorbed H_2O show equally clearly that CH_3OH is also adsorbed in non-Type I sites. The subsequent TPD experiments show that $CH_3O_{(a)}$ species adsorbed at Type I vs. non-Type I sites behave differently. The $CH_3O_{(a)}$ decomposition step occurs 35 K earlier (ca. 2 kcal/mole lower apparent activation energy) at Type I sites, and the resulting $HCOO_{(a)}$ intermediate subsequently decomposes to yield primarily CO, with an apparent activation energy of 40 kcal/mole.

However, it is also important to recognize the converse of this observation, namely that $CH_3O_{(a)}$ species adsorbed in non-Type I sites also decompose cleanly to yield the $HCOO_{(a)}$ intermediate, with an apparent activation energy only 2

kcal/mole greater than for Type I sites. Moreover, evolution of H_2 (as opposed to H_2O) is also observed for the $CH_3O_{(a)}$ decomposition step at non-Type I sites. Since the Type I sites remain blocked by H_2O throughout the $CH_3O_{(a)}$ and $HCOO_{(a)}$ decompositon processes, this indicates that Type I sites are not essential for either CH_3OH decomposition or molecular H_2 desorption from ZnO surfaces.

The origin of the modest enhancement of the $CH_3O_{(a)}$ decomposition kinetics at the Type I sites may be attributed to the enhanced basicity of the $O^=$ anion of the Type I site. A variety of spectroscopic evidence exists to indicate that the Type I sites are located at cation vacancies on the (0001)-Zn polar surface of ZnO[2]. The electrostatic potential at these cation vacancies can be expected to induce a larger proton affinity in the neighboring $O^=$ anions.

Ironically, our hard-won understanding of the behavior of Type I sites now leads us to seriously question the importance of these sites as active participants in the CH_3OH synthesis reaction on Cu/ZnO catalysts. In no case did we observe CH_3OH desorption from $CH_3O_{(a)}$ species adsorbed in Type I sites. We did observe the analogous desorption process for H_2O adsorbed at these sites, but with a desorption energy of 40 kcal/mole, significantly greater than the activation energy for $CH_3O_{(a)}$ decomposition. This large activation energy for recombinative desorption of molecules containing OH groups is also a reflection of the basicity of the Type I $O^=$ anion, and suggests that CH_3OH desorption from Type I sites would be more difficult than from non-Type I sites.

Secondly, the modest enhancement for the $CH_3O_{(a)}$ decomposition step at Type I sites is small, relative to the enhancement for both the $CH_3O_{(a)}$ and $HCOO_{(a)}$ decomposition steps observed when Cu was evaporated onto the ZnO surface. While it does not necessarily follow that the activation energy for the reverse $CH_3O_{(a)}$ synthesis reaciton is also reduced as dramatically, this observation does suggest that the presence of the Cu component will have a more significant influence than the presence of the geometrically distinct Type I sites.

Finally, the large binding energy observed for H_2O in Type I sites suggests that these sites may be blocked under CH_3OH synthesis conditions, since the reactant mixture usually contains added CO_2 that would be converted to H_2O via the reverse shift reaction.

Thus the present results strongly suggest that the origin of the CH_3OH synthesis activity in the Cu/ZnO catalyst does nto reside in the Type I sites found on ZnO. This does not rule out the possibility that analogous sites may be present at isolated Cu cations on the surface of Cu/ZnO catalysts; evidence for the influence of a dispersed Cu species is seen in the Cu/ZnO thin film experiments shown in Figs. 7 and 8. However, the Cu/ZnO experiment also indicate that the $CH_3O_{(a)}$ decomposition activity of the metallic Cu clusters is much greater than for either Type I or non-Type I sites. Moreover, the ZnO support provides a spillover effect which enhances the CH_3OH decompositon activity of the Cu clusters even more, by eliminating the need for pre-exposure to O_2 to provide proton acceptor sites.

ACKNOWLEDGEMENT

This work has been supported by the National Science Foundation, through grant Nos. CPE-8110754 and RIG-CPE-8105823. One of us (D. L. R.) acknowledges stipend support from Chevron Research Company, Standard Oil of California.

REFERENCES

1) I. E. Wachs and R. J. Madix; J. Catal. 53 208 (1978).

2) G. L. Griffin and J. T. Yates, Jr.; J. Chem. Phys. 77 3744, 3751 (1982)

TPD Cell for Transmission - Reflectance Infrared Spectroscopy

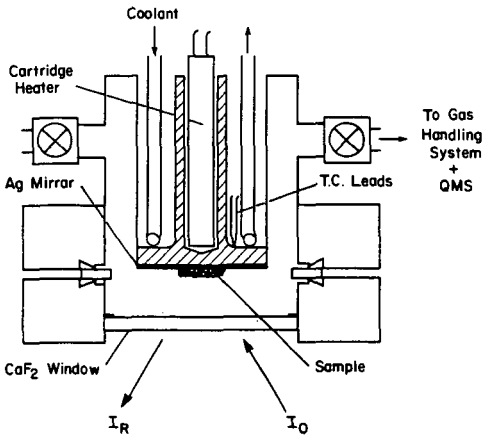

Figure 1. Schematic diagram of sample cell used for combined TPD and IR studies of catalyst powders.

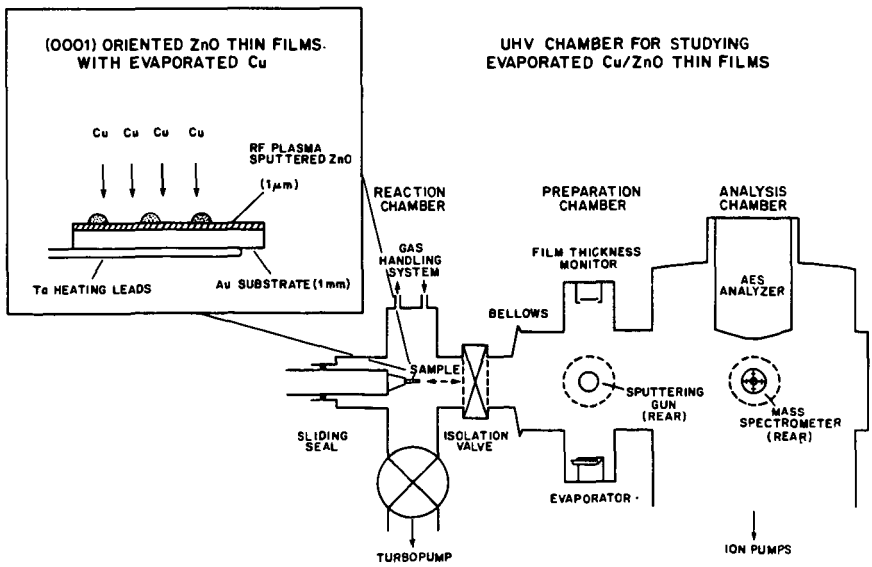

Figure 2. Appartus used for TPD studies on Model Cu/ZnO thin films. Inset: Schematic representation of RF sputtered thin film sample configuration, with in-situ evaporate Cu overlayer.

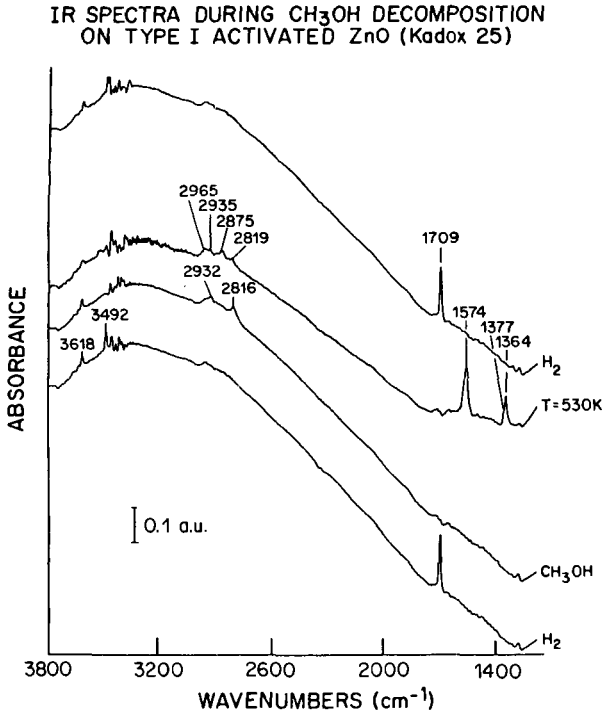

Figure 3. Infrared spectra of CH_3OH and H_2 adsorbed on Type I activated ZnO. Bottom: 40 torr H_2 alone at 300 K. Second: Same sample, exposed to CH_3OH. Third: Same sample after heating to 430 K. Top: Same sample after heating to 673 K, then exposed to 40 torr H_2 at 300 K.

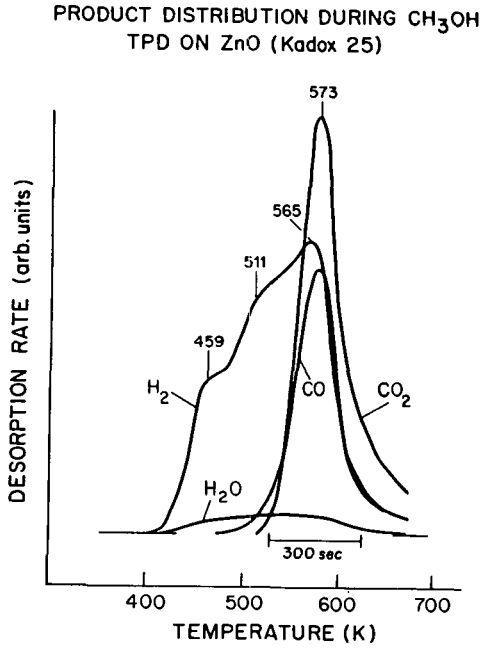

Figure 4. Product distribution spectra during TPD of CH_3OH adsorbed on Type I activated ZnO.

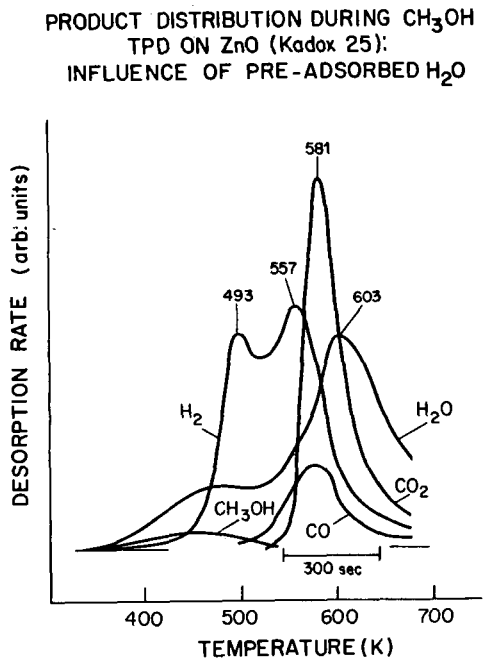

Figure 5. Product distribution spectra during TPD of co-adsorbed CH_3OH and H_2O on ZnO, where H_2O is adsorbed first to block Type I sites.

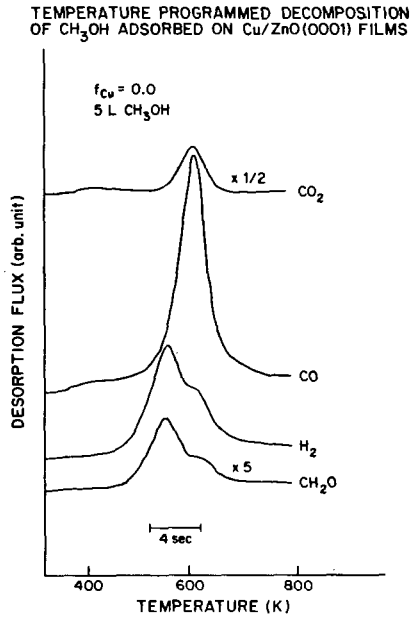

Figure 6. Product distribution spectra during TPD of CH_3OH adsorbed on clean, oriented ZnO thin film.

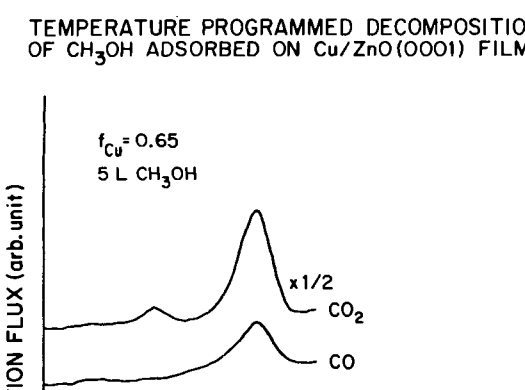

Figure 7. Product distribution spectra during TPD of CH_3OH adsorbed on a Cu/ZnO surface (Auger intensity ratio $I_{Cu}/(I_{Cu} + I_{Zn}) = 0.65$).

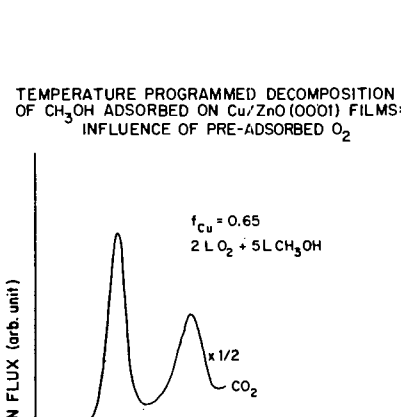

Figure 8. Product distribution spectra during TPD of CH_3OH on Cu/ZnO surface that has been pre-exposed to 2 L of O_2 before CH_3OH adsorption.